

## **FRICITION BEHAVIOR OF ALUMINUM BRONZE REINFORCED BY BORON CARBIDE PARTICLES**

**Alexey Yu. Smolin<sup>1,2</sup>, Andrey V. Filippov<sup>1</sup>, Evgeny V. Shilko<sup>1,2</sup>**

<sup>1</sup>Institute of Strength Physics and Materials Science SB RAS, Tomsk, Russia

<sup>2</sup>National Research Tomsk State University, Tomsk, Russia

**Abstract.** *A promising composite material for tribotechnical applications based on aluminum bronze with reinforcing boron carbide particles fabricated by a special electron beam additive deposition technique was studied experimentally and numerically. Tribological experiments showed that reinforcing by carbide particles allowed reducing the coefficient of friction from 0.26 to 0.19 and improving the wear resistance by 2.2 times. Computer modeling reveals two main factors playing a significant role in the friction behavior of the studied metal matrix composite: the mechanical effect of reinforcing ceramic inclusions and effective hardening of the metal matrix due to the peculiarities of the 3D electron beam printing. The mechanical effect of hardening inclusions determines a more rounded shape of wear particles, preventing wedging, and thereby increasing the stability of friction. Strengthening the metal matrix leads to reducing the number of wear particles.*

**Key words:** *MMC, Aluminum bronze, Boron carbide, Friction, Computer simulation*

### 1. INTRODUCTION

Aluminum bronze is widely used for producing corrosion and wear-resistant products intended for seawater, water supply, and petroleum chemistry applications. Traditional powder metallurgy [1] as well as arc melting technologies [2] are mainly used for this material. The most advanced technologies used for manufacturing products from copper alloys are wire arc additive manufacturing [3, 4], selective laser melting (SLM) [5, 6], and electron beam additive manufacturing (EBAM) [7]. The latest seems the most promising since it needs vacuum and therefore the risk of interlayer oxidizing is excluded. Furthermore, EBAM is more energy-efficient as compared with SLM since no powerful lasers are needed for forming a stable melted pool. To enhance the mechanical properties

---

Received December 26, 2020 / Accepted February 02, 2021

**Corresponding author:** Alexey Smolin

Institute of Strength Physics and Materials Science SB RAS, pr. Akademicheskii 2/4, Tomsk, 634055, Russia

E-mail: [asmolin@ispms.ru](mailto:asmolin@ispms.ru)

of metals they are reinforced by introducing hard inclusions thereby making metal matrix composite (MMC).

For fabricating the copper-based MMC, various powder compounds like oxides, carbides, or antifriction disulfides may be used as fillers [8]. Carbon, as one of the most frequently used fillers, has many disadvantages in tribotechnical applications; one of them is its low resistance to high-temperature oxidizing in the air, which may cause the loss of solid lubricating in high temperature or/and speed loading conditions [9]. Therefore, more stable ceramic materials such as, for example, hexagonal boron nitride or boron carbide are preferable [10]. Boron carbide ( $B_4C$ ) proved to be an effective material for reinforcing MMC [11, 12, 13] as well as for improving the wear resistance of AA7075 [14]. Recently, a special electron beam additive deposition technique was proposed for fabricating an aluminum bronze based MMC filled with  $B_4C$  [15]. Such a composite possesses a gradient distribution of the reinforcing particles and looks very promising for tribotechnical applications.

When developing new materials, it is very useful to have a computational model that could help predict their properties and behavior in the operating conditions. For computer simulation of the mechanical behavior of materials in the friction zone, the numerical methods of computational fluid or/and solid mechanics are usually used [16]. To take into account the elastic-plastic deformation of the main parts of the interacted bodies, as well as stirring of the material in the contact zone, the so-called Arbitrary Lagrangian-Eulerian approach, as well as Smoothed Particle Hydrodynamics, are the most suitable for solving such problems [16, 17, 18]. However, these methods consider the material as a continuum and, therefore, often fail to describe its severe deformation with the accounting of the initial material structure and especially for the formation of new structures in the friction zone. Recently, computational techniques based on particle mechanics have been rapidly developed and utilized for such phenomena. Among them, we would like to point out the Discrete Element Method and Movable Cellular Automaton method as the most promising ones [19, 20].

Thus, the main purpose of this paper is to study the peculiarities of sliding friction behavior of novel aluminum bronze based composites filled with  $B_4C$  reinforcing particles fabricated by additive electron beam deposition method and to develop a computational particle-based model for numerical studying friction and wear of such heterogeneous materials.

## 2. EXPERIMENTAL STUDY

### 2.1. Materials and methods

The samples studied here experimentally were printed using an electron beam additive deposition technique that was described in [21]. A sequential application of aluminum bronze Cu-7.5wt%Al wire-feed and  $B_4C$ +Al powder-bed electron beam methods were used for preparing gradient heterogeneous CuAl- $B_4C$  samples [15]. Two  $(B_4C)_xAl_{1-x}$  powder mixtures with different boron carbide/aluminum bronze weight ratios  $x$  corresponding to  $(B_4C)_{0.5}Al_{0.5}$  (Sample 1) and  $(B_4C)_{0.25}Al_{0.75}$  (Sample 2), respectively, were prepared and then sequentially deposited on a previously deposited Cu-7.5 wt%Al

alloy layers. To prepare the powder mixtures, a boron carbide powder with an average particle size of  $\sim 200 \mu\text{m}$  and an aluminum powder with an average particle size of  $\sim 5 \mu\text{m}$  were used.

The microhardness of the manufactured samples was measured using a «Duramin-5» (Stuers ApS, Denmark) microhardness tester at 50 N load. It was shown that mechanical strength and hardness of the Cu-7.5 wt%Al matrix were enhanced by incorporating carbide particles as follows from the dependencies of microhardness on the distance below the surface, which correlate with the content of  $\text{B}_4\text{C}$  [15]. The maximum  $>1.25 \text{ GPa}$  gain in hardness was observed at a distance of  $\sim 1.2 \text{ mm}$  below the surface, i.e. down to the middle part of the CuAl- $\text{B}_4\text{C}$  samples. The microhardness of Sample 1 with higher boron carbide content is increased more sharply as compared to that of Sample 2. The maximum hardness numbers of Samples 1 and 2 are 4.63 GPa and 2.35 GPa, respectively. The bottom parts of both CuAl- $\text{B}_4\text{C}$  samples possess microhardness negligibly higher than that of Cu-7.5 wt%Al matrix.

Samples for tribological experiments were prepared from the additively manufactured CuAl- $\text{B}_4\text{C}$  samples by cutting them by planes normal to the printed layers. The referenced pure metallic samples were cut off from the deposited Cu-7.5 wt%Al alloy samples. All the samples were mechanically ground on an emery paper to reach the final roughness of  $R_a = 2.5 \mu\text{m}$ . A tribometer Tribotester (TRIBOtechnic, France) was operated in a reciprocal sliding mode with 3 Hz frequency during 105 cycles; the study was performed in accordance with ASTM G-133 standard. Standard 52100 bearing steel 6 mm diameter ball was used as a counterbody. The normal load on the ball was 22 N, which corresponded to a mean contact pressure of about 25 MPa. During the tribological tests, the temperature was  $25^\circ\text{C}$  and humidity 45%. We performed three tests per sample.

Metallographic structures and worn surfaces were examined using a confocal laser scanning microscope LEXT 4100 (Olympus, Japan) and scanning electron microscope (SEM) Tescan MIRA 3 LMU (Tescan, Czech Republic) attached with the add-on for Energy-dispersive X-ray spectroscopy (EDS).

## 2.2. Results

The highest coefficient of friction (CoF)  $\sim 0.26$  was demonstrated at sliding of a  $\text{B}_4\text{C}$ -free Cu-7.5 wt%Al metal against a steel ball (Fig. 1a). Reinforcing the matrix metal with boron carbide particles allowed reducing the CoF to  $\sim 0.23$  and  $\sim 0.19$  for Samples 1 and 2, respectively, i.e. higher content of boron carbide and higher microhardness of Sample 1 provided sliding with a coefficient of friction higher than that of Sample 2. The reason may be more severe abrading the steel ball surface by pulled-out  $\text{B}_4\text{C}$  particles.

Quantification of wear performed by determining the wear groove cross-section area (Fig. 1b) allows concluding that the total wear of Sample 2 was minimal with the value as low as  $2.16 \times 10^{-3} \mu\text{m}^2$ , i.e. of  $\sim 19\%$  lower than that of Sample 1 ( $2.67 \times 10^{-3} \mu\text{m}^2$ ) and of  $\sim 2.2$  times lower than that of Cu-7.5 wt%Al. The wear of Sample 1 was 1.75 times lower than that of Cu-7.5 wt%Al. Maximum wear groove depths were 39  $\mu\text{m}$ , 34  $\mu\text{m}$ , and 64  $\mu\text{m}$ , for Samples 1, 2, and Cu-7.5 wt%Al correspondingly.

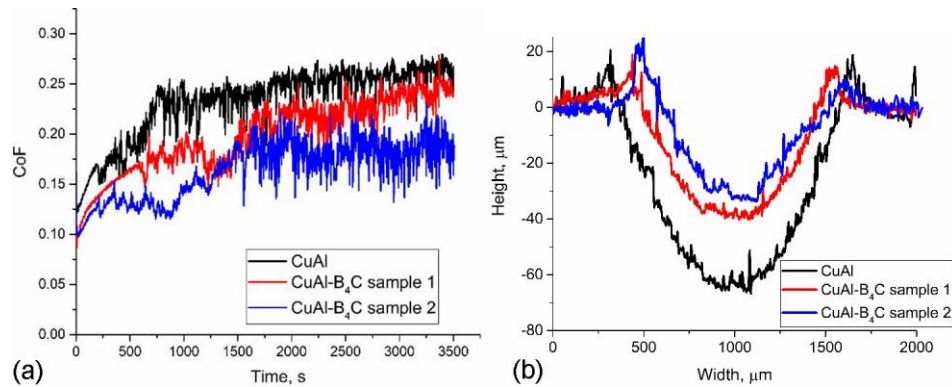


**Fig. 1** Time dependencies of the coefficient of friction for deposited metal and composite samples (a) and their wear groove cross-section profiles (b)

The worn surfaces of all the samples were represented by wear grooves of different depths and widths formed by the material removal. The wear groove surfaces of all samples were covered by red-brown patch areas identified as oxidized areas, mechanically mixed layers (MML) formed by adhesion transfer, and some amount of black wear debris. SEM back scattering electron (BSE) images of the worn surfaces demonstrate at least three areas with different BSE contrast levels (the images for Sample 1 are shown in Fig. 2, for example): bright, dark, and black.

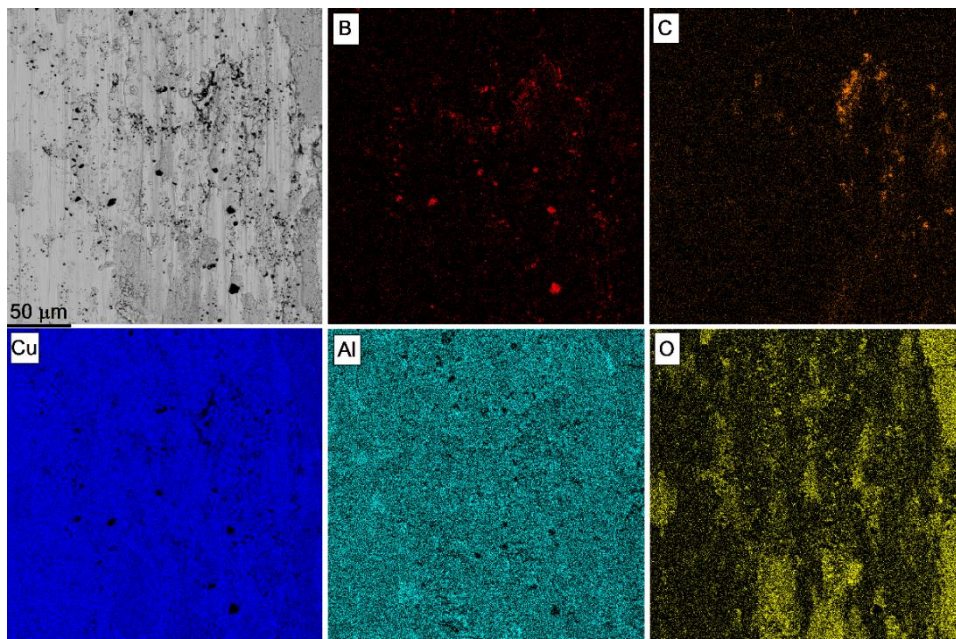


**Fig. 2** SEM BSE image and EDS element maps of the worn surface of Sample 1

According to EDS element maps shown in Fig. 2 bright areas in the SEM BSE image correspond to less oxidized layers (see maps for O), while the darker ones represent high oxygen areas. Black particles or agglomerates correspond to boron carbides (see maps for B and C in Fig. 2) and were detected on the worn surfaces of Samples 1 and 2. At the same time, the B-enriched particles do not always coincide with the C-enriched ones in Fig. 2 what may be evidence in favor of boron carbide decomposition in the melted pool under electron beam irradiation. Therefore, at least part of the black particles in the worn surfaces may be free carbon black ones.

Mechanically mixed layers composed of wear debris and oxides were found on all samples when examining the sample sections by the planes parallel to the sliding direction and perpendicular to the sample surface (Fig. 3, this pictures also depict the spatial distribution of reinforcing boron carbide particles in the composite samples). The MML with a thickness of 22  $\mu\text{m}$  was generated on the most ductile Cu-7.5 wt%Al sample (Fig. 3a) while thicknesses of 7  $\mu\text{m}$  and 13  $\mu\text{m}$  were obtained on the hardest CuAl-B<sub>4</sub>C Sample 1 and less hard Sample 2, respectively (Fig. 3b and c). These results look reasonable since the higher hardness of Sample 1 means less ductility and less penetration of plastic deformation into the sample. Therefore, only thin MMLs may be generated by subsurface plastic deformation in hard materials.

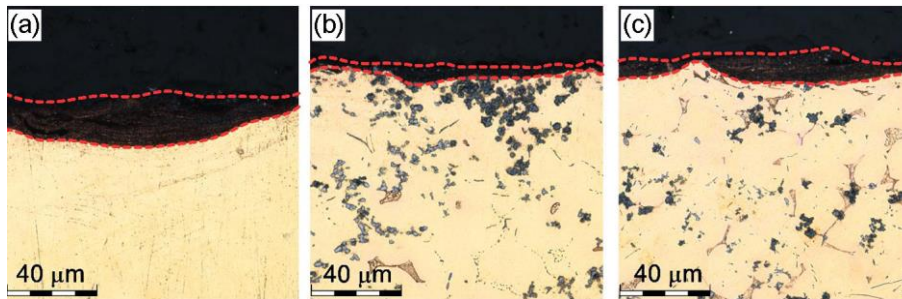


**Fig. 3** Longitudinal cross-sections of wear grooves with MML layers on Cu-7.5 wt%Al (a), CuAl-B<sub>4</sub>C Sample 1 (b), and Sample 2 (c)

### 3. COMPUTER SIMULATION

#### 3.1. Model description

The numerical model of sliding friction used herein is based on the method of movable cellular automata (MCA), which is a representative of simply deformed discrete element method, i.e. particle mechanics, which looks very promising for the simulation of heterogeneous materials at mesoscale, where the structure has to be considered explicitly [20, 22, 23]. In this method, it is assumed that any material consists of a certain number of discrete elements (called movable cellular automata) of a finite size that can move, rotate, and change their state due to interaction with neighbors thereby simulating real deformation and physical processes. The motion of the elements is governed by Newton-Euler equations. The force acting between the automata is written in the many-body form

and defined by the local strain parameters and usual moduli of elasticity. In plastic flow, the dependence of the inter-automata force on strain is defined by the local stress-strain curve of the material, which is called the response function of the automaton. Actually, the plastic flow theory using the von Mises criterion is adopted for modeling plasticity in MCA. A pair of automata can be in one of two possible states: bonded and unbonded. Thus, in MCA, fracture and coupling of fragments (crack healing, cold micro-welding, etc.) are simulated by the corresponding switching of the pair state. Switching criteria depend on the physical mechanisms of material behavior.

It worth noting, that the MCA method has been successfully being used for the simulation of friction for about 20 years. Thus, the main model and corresponding software have been validated for modeling the elastoplastic behavior of metallic materials in contact loading and friction (see, for example, [24]). The novelty of the model used herein consists in the new fracture criterion defined by the ultimate value of the strain energy, and the new algorithm and criterion for automata coupling (considered as a process, which takes several time steps) defined by the plastic heat value combined with the condition of compression [23]. Besides, in the used MCA-model such physical phenomena as thermo-elasticity and heat transfer are also implemented.

Herewith we model the metal matrix composite based on aluminum bronze with reinforcing boron carbide inclusions. The properties of the components were obtained from the literature, namely, the elastoplastic properties of the bronze matrix were taken from [25, 26], while the elastic-brittle properties for the carbide inclusions from [27].

Mechanical and thermophysical properties of aluminum bronze: density  $7800 \text{ kg/m}^3$ , Young's modulus  $118 \text{ GPa}$ , Poisson's ratio  $0.295$ , yield strength  $360 \text{ MPa}$ , tensile strength  $560 \text{ MPa}$ , coefficient of linear thermal expansion  $1.78 \cdot 10^{-5} \text{ K}^{-1}$ , specific thermal conductivity  $80 \text{ W/(m}\cdot\text{K)}$ , specific heat  $418 \text{ J/(kg}\cdot\text{K)}$ . The plastic heat value used as a criterion for coupling the bronze automata is  $141 \text{ J/m}^3$  combined with a condition of compressive stress of  $360 \text{ MPa}$ .

Properties of  $\text{B}_4\text{C}$ : density  $2510 \text{ kg/m}^3$ , Young's modulus  $440 \text{ GPa}$ , Poisson's ratio  $0.17$ , ultimate compressive strength  $5680 \text{ MPa}$ , tensile strength  $2270 \text{ MPa}$ , coefficient of linear thermal expansion  $0.4 \cdot 10^{-5} \text{ K}^{-1}$ , specific thermal conductivity  $40 \text{ W/(m}\cdot\text{K)}$ , specific heat  $1200 \text{ J/(kg}\cdot\text{K)}$ .

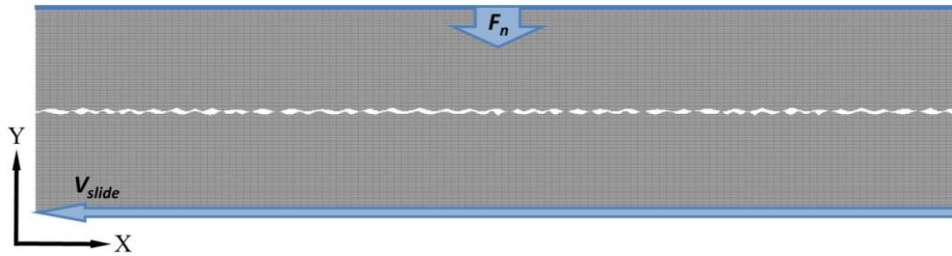


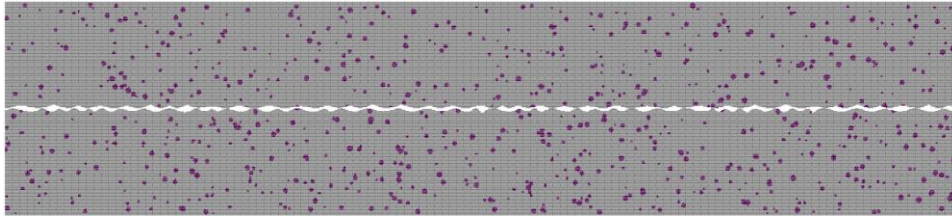
**Fig. 4** View of 2D sample for modeling friction and scheme of its loading

Two contacting rough surfaces of metallic materials with the same properties were modeled, mimicking a mesoscopic fragment of the friction contact zone of macroscopic bodies (Fig. 4). In 2D formulation, the approximation of a plane-stress or plane-strain

state was used. The linear dimensions of the model were  $L = 1000 \mu\text{m}$  along the  $X$ -axis and  $H = 220 \mu\text{m}$  along the  $Y$ -axis. The size of the discrete element was  $d = 1 \mu\text{m}$ . The surface of each of the contacting bodies (hereinafter referred to as blocks) contains more than 40 asperities. The average distance between asperities  $S_{\text{mi}} = 23 \mu\text{m}$ , maximum profile height  $R_{\text{max}} = 5 \mu\text{m}$ .

The friction of the blocks was simulated by their relative tangential displacement at a constant speed and a given constant value of the contact pressure  $\sigma_n = 36 \text{ MPa}$ , which was set by applying a force  $F_n$  to the upper surface of the upper block (Fig. 4). The  $x$ -coordinates of the elements of the upper surface of the sample were fixed. The base of the system (the lower surface of the lower block) was fixed in the  $Y$  direction and moves along the  $X$ -axis at a constant velocity  $V_{\text{slide}} = 5 \text{ m/s}$ .

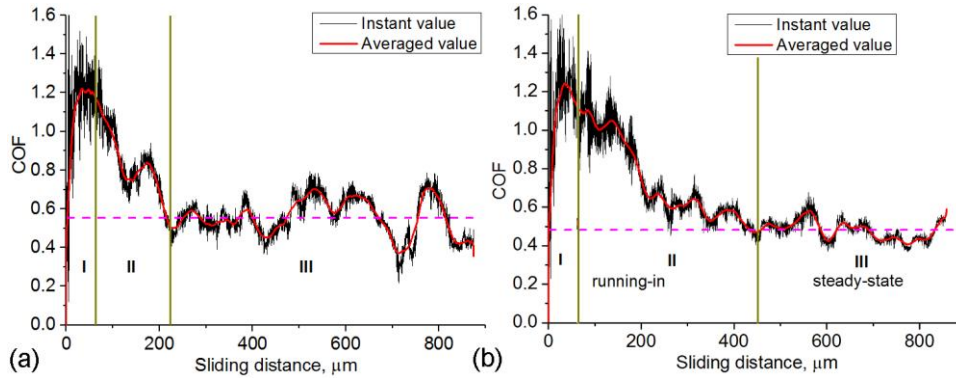
To reveal the influence of boron carbide inclusions on the friction behavior of the aluminum bronze, we model the pure bronze samples as well as composite samples. Fig. 5 shows an example of the structure of a model composite material with a matrix of aluminum bronze and 5 vol. % of dispersed ceramic inclusions. The inclusions are represented by both individual elements ( $1 \mu\text{m}$  in size) and agglomerates of these elements up to  $6\text{--}8 \mu\text{m}$  in size.



**Fig. 5** 2D sample for modeling friction of MMC with 5% of  $\text{B}_4\text{C}$  inclusions

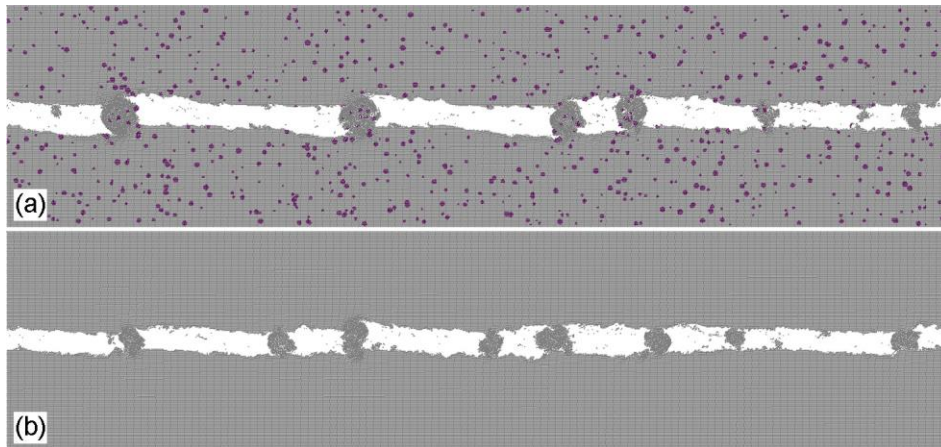
### 3.2. Results of computer simulation

Fig. 6 shows the time dependencies of the friction coefficient change for the samples of pure bronze and composite for the case of the plane-stress state. The similarity of these curves can be noted; the length of the initial stage of the growth of the friction coefficient to values above 1 corresponds approximately to each other. At the same time, the transitional stage in the development of the friction, accompanied by a multiple decreases in the coefficient of friction, is almost three times longer for the composite than for pure bronze. It consists of two stages: the stage of a rapid decrease in the coefficient of friction and the stage of a smooth transition of the coefficient of friction to a steady value, which is approximately equal in length. It is also important to note two main points at the stage of the steady-state friction of the composite: i) the average value of CoF ( $\sim 0.48$ ) is significantly lower than that of pure bronze ( $\sim 0.55$ ); ii) the characteristic amplitude of CoF variation is also significantly lower.



**Fig. 6** Time dependence of the instantaneous CoF on the relative tangential displacement of the blocks. The red line depicts averaging the instantaneous values in a window of 100 points

Analysis of the simulation results showed that these differences are associated with the peculiarities of the formation of wear particles in the composite material. Indeed, already at the stage of running-in, the process of formation of new contact spots on wear particles proceeds much faster (Fig. 7). In particular, the presence of relatively large  $B_4C$  particles leads to the adhesion of additional surface layers of the material on them. This is due to the fact that hard ceramic particles are stress concentrators. Therefore, more intense strain localization occurs in the adjacent matrix layer, which leads to the rapid formation of local interface cracks. Ceramic particles detached from the blocks carry with them a matrix layer of the corresponding thickness. Or, being on the surface of wear particles, they act on the adjoining surface of the blocks as indenters and abrasives. The result of these effects is, in addition to accelerating the growth of wear particles, their more rounded shape.



**Fig. 7** 2D sample for modeling friction of MMC (a) and aluminum bronze (b) at friction path  $l_x=240 \mu\text{m}$  (correspond to the end of stage II in Fig. 6)

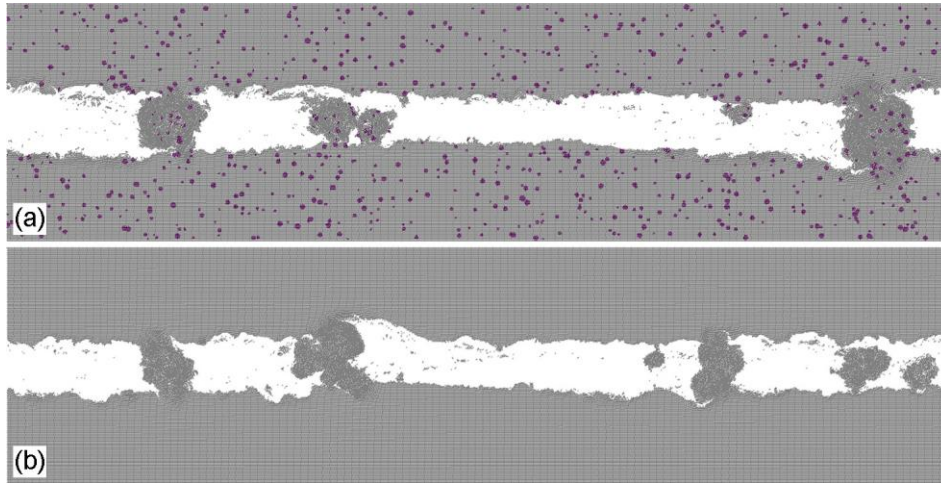


**Fig. 8** 2D sample for modeling friction of MMC with 5% of  $B_4C$  inclusions at friction path  $l_x=650 \mu m$

At the steady-state stage, the rounded shape of the wear particles (Fig. 8) prevents wedging in the contact zone and thereby helps to reduce the amplitude of fluctuations in the coefficient of friction. At the same time, the weak adhesion of the particles to the surfaces (due to the interface zones of ceramic inclusions with bronze, the formation of cracks in which occurs earlier than in the bulk of the bronze matrix), determines a significant decrease in the overall level of the friction coefficient.

Note that the features of the friction model of aluminum bronze described in [23] (the formation of large wedges/prows and a high coefficient of friction) under mechanically constrained conditions of a plane-strain state are also valid for material with carbide inclusions. In this case, the value of the coefficient of friction for such material ( $\sim 1.2-1.3$ ) is even slightly higher than that for pure aluminum bronze. This allows us to assume that the differences in the values of the friction coefficient of the bronze and the composite in the 3D case will be less than in the case of a mechanically unconstrained system considered here (plane-stress state).

### 3.3. Role of the mechanical characteristics of the matrix in the friction of MMC

The presented simulation results allow a better understanding of the mechanisms that are able to determine the effect of reducing the friction coefficient obtained in an experimental study in the material with a gradient structure fabricated by the method of electron-beam deposition (by approximately 0.05 in comparison with aluminum bronze).

Indeed, the experimentally established change in the friction coefficient in a material with a gradient composite structure ( $CuAl-B_4C$ ), obtained by electron-beam deposition, can be caused not only by the mechanical effect of inclusions but also by a change in the mechanical characteristics of the bronze matrix [15]. These changes can be determined by the following factors:

1) In the process of cooling the crystallized composite from the melting point to room temperature, “additional” geometrically necessary dislocations (GNDs) are formed in the layer of the metal matrix surrounding the surface of the ceramic particles. The density of these dislocations can be an order of magnitude higher than the density of dislocations far from the surface of the inclusions. An increase in the dislocation density provides an increase in the yield stress of the interface layer of the matrix.

2) An additional increase in the density of the GNDs in the interface layer of the matrix can also be achieved during deformation of the composite material due to the difference in elastic moduli and plastic properties of the phases and, as a consequence, a high gradient of deformations at the interface. This effect provides an effective increase in the strain-hardening coefficient of the interface zone.

3) Carbide particles can partially dissolve in the molten bronze, which can lead to the appearance of impurities of the corresponding chemical elements in the crystal lattice of the matrix and cause an increase in its yield stress and, possibly, the coefficient of strain hardening.

To study the influence of the first two factors, a theoretical assessment of the increase in the yield point and the coefficient of deformation hardening of the considered aluminum bronze was carried out. The influence of the first of them is assessed on the basis of the relationships proposed by Shibata [28]:

$$\sigma'_y = \sigma_y + aGb\sqrt{\rho_{\text{therm}}}, \quad (1)$$

where:

$$\rho_{\text{therm}} = \frac{12\sqrt{2}\Delta_{\text{CTE}}\Delta T}{bd_p} \frac{F_p}{1-F_p}, \quad (2)$$

here  $\sigma'_y$  is the value of the yield stress of the bronze matrix, taking into account the GNDs that have arisen during cooling ( $\sigma_y = 360$  MPa),  $a$  is the dimensionless Taylor coefficient,  $G$  and  $b$  are the shear modulus and the Burgers vector,  $\rho_{\text{therm}}$  is the density of thermally induced GNDs,  $\Delta_{\text{CTE}}$  is the difference in the value of the coefficient of thermal expansion of the matrix and inclusion,  $\Delta T$  is the difference between the melting point of bronze and room temperature,  $F_p = (r/R)^3$ , where  $r$  and  $R$  are half the average particle size of inclusions  $d_p$  and half the average distance between the particles. Note that the effect of thermally induced GNDs on the loading diagram is taken into account by “raising” the unified hardening curve by  $\Delta\sigma_y = \sigma'_y - \sigma_y$ .

The influence of the second factor (an increase in the strain hardening coefficient) was estimated based on the relations of the nonlocal theory of plasticity by H. Gao and Y. Huang [29]

$$\sigma'(\epsilon_p) = \sqrt{|\sigma(\epsilon_p)|^2 + 27\sqrt{5/2}G^2\eta^2 b/r\epsilon_p\sqrt[3]{f}}, \quad (3)$$

where  $\sigma(\epsilon_p)$  is the curve of uniaxial loading of the material in terms of plastic axial deformation  $\epsilon_p$  taking into account the correction  $\Delta\sigma_y$  from Eq. (1) due to thermally induced GND,  $f$  is the volume fraction of inclusions,  $\eta$  is the dimensionless coefficient of the model.

The performed estimates show that for the material under consideration, the main influence on the change in the mechanical properties of the composite should be provided

by the GNDs arising during cooling from the melt. The influence of GNDs arising during deformation due to "plastic inconsistency" is a factor of a smaller order of magnitude (black and blue curves in Fig. 9).

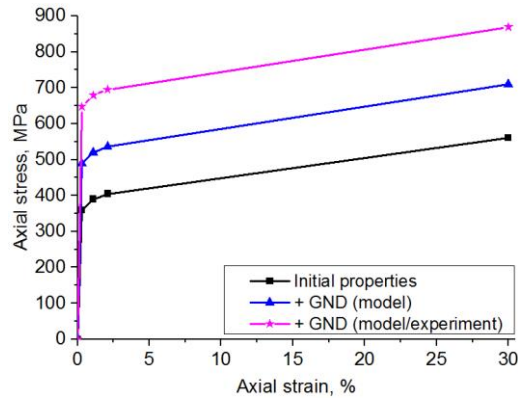


**Fig. 9** Piecewise linear approximation of the experimental diagram of uniaxial tension of a sample of aluminum bronze (black curve) and diagrams of a hardened bronze matrix due to GND, estimated theoretically (blue curve) and experimental+theoretically (lilac curve)

Note that the above-described increase in the GND occurs only in the interface layer of the matrix, the thickness of which is estimated theoretically based on the linear dimensions of inclusions, their concentration, the characteristic distance between them, the mechanical and atomic characteristics of the phases, etc. [28]. Due to the current lack of comprehensive quantitative experimental information on the characteristics of the distribution of  $B_4C$  inclusions, in the calculations presented below, an "upper estimate" is used, which assumes that the entire volume of the bronze matrix is subjected to dislocation hardening (as the parameter  $R$  in Eq. (2), half of the average distance between the inclusions).

When conducting compression tests of small samples of the experimentally obtained material with a gradient structure (in a layer with a  $B_4C$  content of ~9 vol.%; this volume concentration approximately corresponds to a two-dimensional concentration of 5-6%, which is considered in our calculations), it was found that its yield point is approximately 1.8 times higher than that of the aluminum bronze samples. This significantly exceeds the theoretically estimated value and may be due to the presence of impurity atoms. At the same time, the experimentally determined strain-hardening coefficient of the obtained material increased insignificantly in comparison with aluminum bronze and correlates well with the estimates according to Eq. (3). In fact, the difference between the experimental and theoretically estimated data on the hardening curve of a composite material obtained by electron beam deposition consists in the difference in the value of the yield stress. To assess the effect of this parameter, a modified matrix is also considered (lilac curve in Fig. 9), in which the value of the yield stress corresponds to the experimentally determined value, and the strain-hardening coefficient is modified according to Eq. (3).

For model composites with modified matrices, friction was simulated under the same loading conditions as in the previous cases considered. The new value of yield stress was considered as the minimum contact pressure at which the coupling of the corresponding automata is possible.

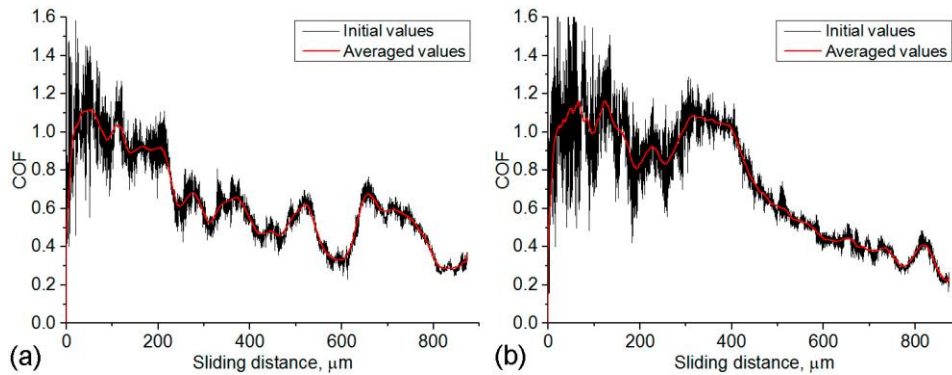


**Fig. 10** The dynamics of the instantaneous friction coefficient in a pair of blocks of the composite material: a) taking into account the strengthening of the matrix due to the GNDs estimated theoretically; b) taking into account the strengthening of the matrix due to GNDs estimated based on the analysis of experimental data (thermally induced GND) and theoretically (GNDs due to “plastic inconsistency” of the phases)

Fig. 10 shows the change in the coefficient of friction for the samples with modified matrices under conditions of a plane-stress state. It can be noted that an increase in the yield point leads to the following changes.

1) The length of the running-in stage increases significantly. In the problems considered, the value of the relative tangential displacement of the blocks was approximately equal to the length of the system (about 1 mm). Nevertheless, this turned out to be insufficient for reaching the steady-state regime.

2) The friction coefficient decreases with the increase in the yield point (Figs. 6 and 10). In particular, an increase in the yield stress of the matrix by 1.8 times is accompanied by a decrease in the steady-state coefficient of friction by at least 0.1 in comparison with a composite material with the original matrix.

The noted differences are associated with the peculiarities of the formation of wear particles in a composite material with a hardened matrix (Fig. 11). So, already at the initial stage of running-in (after cutting and/or smoothing the initial asperities of the surface), the number of new contact spots (wear particles) is several times lower than in the samples with the unmodified matrix. At the same time, the higher the yield point, the lower the number of formed wear particles at the initial stage of friction. So, in Fig. 11, corresponding to the hardest matrix, one can see the formation of only two wear particles, which later determine the dynamics of change in the friction coefficient and wear. The reason for this effect is an increase in the “bonding threshold” of materials due to an increase in the yield stress (the contact pressure required for coupling the matrix automata). In this case, only those initial fragments of the “third body” begin to grow, in

which the local contact pressure is sufficient for cold welding with the rest materials surface. With an increase in the yield point, such spots become less and less, which determines the formation of a small number of wear particles. Thus, in contrast to the original aluminum bronze (or a composite with a matrix with initial mechanical properties), in the case of a hardened matrix, the initially formed wear particles are stable and long-lived formations that determine the further development of friction and wear processes.

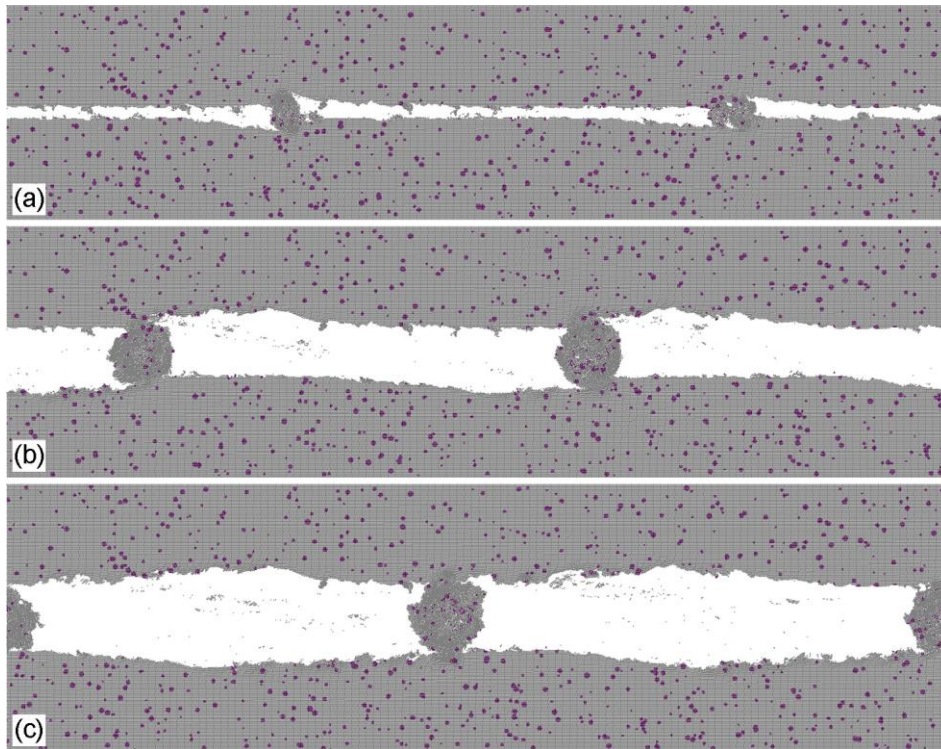


**Fig. 11** The structure of the contact zone of the blocks of the composite material at different times of friction: (a)  $lx = 275 \mu\text{m}$ ; (b)  $lx = 575 \mu\text{m}$ ; (c)  $lx = 870 \mu\text{m}$ ; the mechanical properties of the matrix correspond to the lilac curve in Fig. 9

Note also that the result obtained correlates with the discussion in [30, 31] of the features of shaping prows/wedges in a variety of materials. Indeed, as shown in this work, the linear dimensions and stability (duration) of the existence of prows/wedges in friction pairs are largely determined by the mechanical parameters of the materials, first of all, by the hardness, which is largely determined by the yield point. The simulation results allowed us to offer one of the possible explanations for this feature.

#### 4. CONCLUSION

Friction and wear of the aluminum bronze based composites with reinforcing boron carbide particles fabricated by a combination of wire-feed and powder-bed electron beam deposition methods were studied experimentally. It was shown that reinforcement of the aluminum bronze matrix with  $B_4C$  particles allowed improving the wear resistance of the composites as compared to that of pure aluminum bronze deposited. Coefficient of friction reduced from 0.26 to 0.19. The composite of composition  $(B_4C)_{0.25}Al_{0.75}$  showed its wear resistance by a factor of 2.2 higher as compared to that of printed Cu-7.5 wt% Al bronze.

Using computer modeling, the factors have been identified that have a significant effect on the value of the coefficient of friction of metal matrix composite based on aluminum bronze and reinforced by boron carbide particles. These factors include the mechanical effect of reinforcing ceramic inclusions and effective hardening of the metal matrix due to the peculiarities of the 3D electron beam printing process. It is shown that the mechanical effect of hardening inclusions determines a more rounded shape of wear particles, preventing wedging, and thereby increasing the stability of the friction coefficient. At the same time, the weaker integral adhesion of wear particles to the surfaces contributes to a slight decrease in the coefficient of friction. Strengthening the metal matrix leads to reduce the number of wear particles and therefore is a factor in determining the overall level of the coefficient of friction.

Thus, the results of computer modeling presented herein confirm the supposition derived from the experimental evidence that electron beam additive manufacturing of CuAl- $B_4C$  composite leads to additional reinforcing of the aluminum bronze matrix by boron carbide dissociation and precipitation. So, when contacting the copper melt bead, the boron carbide may dissociate into boron and carbon; boron then may dissolve in copper and form Cu-B eutectics while carbon stays free in the form of the black particle [15]. The simulation results also confirm that the higher friction coefficient of pure bronze may be explained by the higher adhesion of this material, while the presence of carbide and carbon particles reduces the adhesion and consequently the value of friction coefficient.

The results obtained are relevant, in particular, for solving problems of friction and wear control in materials with a gradient internal structure by choosing the optimal 3D printing modes.

**Acknowledgement:** *The study was carried out with the financial support of the Russian Science Foundation (Project No. 20-19-00743). The authors would like to thank A.S. Grigoriev for his help in performing calculations and preparing the figures.*

#### REFERENCES

1. Shaik, M.A., Golla, B.R., 2019, *Development of highly wear resistant Cu-Al alloys processed via powder metallurgy*, Tribology International, 136, pp. 127-139.
2. Liu, X., Ohnuma, I., Kainuma, R., Ishida, K., 1998, *Phase equilibria in the Cu-rich portion of the Cu-Al binary system*, Journal of Alloys and Compounds, 264, pp. 201-208.

3. Dong, B., Pan, Z., Shen, C., Ma, Y., Li, H., 2017, *Fabrication of copper-rich Cu-Al alloy using the wire-arc additive manufacturing process*, Metallurgical and Material Transactions B Process Metallurgy and Materials Processing Science, 48, pp. 3143-3151.
4. Wang, Y., Chen, X., Kononov, S., Su, C., Siddiquee, A.N., Gangil, N., 2019, *In-situ wire-feed additive manufacturing of Cu-Al alloy by addition of silicon*, Applied Surface Science, 487, pp. 1366-1375.
5. Feng, X., Cui, X., Jin, G., Zheng, W. Cai, Z., Wen, X., Lu, B., Liu, J., 2018, *Underwater laser cladding in full wet surroundings for fabrication of nickel aluminum bronze of coatings*, Surface and Coatings Technology, 333, pp. 104-114.
6. Tao, X.P., Zhang, S., Wu, C.L., Zhang, C.H., Zhang, J.B., Liu, Y., 2018, *Thermal stability and corrosion resistance in a novel nickel aluminum bronze coating by laser cladding*, Materials Research Express, 5, 116527.
7. Wolf, T., Fu, Z., Körner, C., 2019, *Selective electron beam melting of an aluminum bronze: microstructure and mechanical properties*, Materials Letters, 238, pp. 241-244.
8. Gautam, Y.K., Somani, N., Kumar, M., Sharma, S.K., 2018, *A review on fabrication and characterization of copper metal matrix composite (CMMC)*, AIP Conference Proceedings, 2018, 020017.
9. Mutterle, P.V., Cristofolini, I., Pilla, M., Pahl, W., Molinari, A., 2011, *Surface durability and design criteria for graphite-bronze sintered composites in dry sliding applications*, Materials and Design, 32, pp. 3756-3764.
10. Maruyama, T., Onose, S., 1999, *Fabrication and thermal conductivity of boron carbide/copper cermet*, Journal of Nuclear Science and Technology, 36(4), pp. 380-385.
11. Ramnath, B.V., Elanchezian, C., Jaivignesh, M., Rajesh, S., Parswajinan, C., Ghias, A.S.A., 2014, *Evaluation of mechanical properties of aluminium alloy-alumina boron carbide metal matrix composites*, Materials and Design, 58, pp. 332-338.
12. Tuncer, A., Tasdelen, B., Arslan, G., 2011, *Effect of passivation and precipitation hardening on processing and mechanical properties of B<sub>4</sub>C-Al composites*, Ceramics International, 37, pp. 2861-2867.
13. Fomin, V.M., Golyshv, A.A., Kosarev, V.F., Malikov, A.G., Orishich, A.M., Filippov, A.A., 2020, *Deposition of cermet coatings on the basis of Ti, Ni, WC, and B<sub>4</sub>C by cold gas dynamic spraying with subsequent laser irradiation*, Physical Mesomechanics, 23, pp. 291-300.
14. Shin, S., Lee, D., Lee, Y.-H., Ko, S., Park, H., Lee, S.-B., Cho, S., Kim, Y., Lee, S.-K., Jo, I., 2019, *High temperature mechanical properties and wear performance of B<sub>4</sub>C/Al7075 metal matrix composites*, Metals, 9, 1108.
15. Filippov, A.V., Khoroshko, E.S., Shamarin, N.N., Savchenko, N.L., Moskvichev, E.N., Utyaganova, V.R., Kolubaev, E.A., Smolin, A.Yu., Tarasov, S.Yu., 2021, *Characterization of gradient CuAl-B<sub>4</sub>C composites additively manufactured using a combination of wire-feed and powder-bed electron beam deposition methods*, Journal of Alloys and Compounds, in press, article 157824. <https://doi.org/10.1016/j.jallcom.2020.157824>
16. He, X., Gu, F., Ball, A., 2014, *A review of numerical analysis of friction stir welding*, Progress in Materials Science, 65, pp. 1-66.
17. Sanjeev, N.K., Ravikiran, B.P., 2015, *Application of coupled Eulerian Lagrangian approach in finite element simulation of friction stir welding*, Simulia Community Conference Proceedings May 18-21, 2015 Berlin, Germany, pp. 1062-1079.
18. Pan, W., Li, D., Tartakovsky, A.M., Ahzi, S., Khraisheh, M., Khaleel, M., 2013, *A new smoothed particle hydrodynamics non-Newtonian model for friction stir welding: Process modeling and simulation of microstructure evolution in a magnesium alloy*, International Journal of Plasticity, 48, pp.189-204.
19. Terreros, I., Iordanoff, I., Charles, J.L., Coupard, D., Tcherniaieff, S., 2009, *Discrete element method, a tool to investigate complex thermo mechanical behaviour: application to friction stir welding*, International Journal of Material Forming, 2, pp. 573-576.
20. Smolin, A.Yu., Shilko, E.V., Astafurov, S.V., Kolubaev, E.A., Eremina G.M., Psakhie, S.G., 2018, *Understanding the mechanisms of friction stir welding based on computer simulation using particles*, Defence Technology, 14, pp. 643-656.
21. Utyaganova, V.R., Filippov, A.V., Shamarin, N.N., Vorontsov, A.V., Savchenko, N.L., Fortuna, S.V., Gurianov, D.A., Chumaevskii, A.V., Rubtsov, V.E., Tarasov, S.Y., 2020, *Controlling the porosity using exponential decay heat input regimes during electron beam wire-feed additive manufacturing of Al-Mg alloy*, International Journal of Advanced Manufacturing Technology, 108, pp. 2823-2838.

22. Shilko, E.V., Psakhie, S.G., Schmauder, S., Popov, V.L., Astafurov, S.V., Smolin, A.Yu., 2015, *Overcoming the limitations of distinct element method for multiscale modeling of materials with multimodal internal structure*, Computational Materials Science, 102, pp. 267-285.
23. Psakhie, S., Shilko, E., Smolin, A., Astafurov, S., Ovcharenko, V., 2013, *Development of a formalism of movable cellular automaton method for numerical modeling of fracture of heterogeneous elastic-plastic materials*, Frattura ed Integrità Strutturale, 7(24), pp. 26-59.
24. Bucher, F., Dmitriev, A.I., Ertz, M., Knothe, K., Popov, V.L., Psakhie, S.G. Shilko, E.V., 2006, *Multiscale simulation of dry friction in wheel/rail contact*, Wear, 261, (7-8), pp. 874-884.
25. Yin, Z., Sun, L., Yang, J., Gong, Y., Zhu, X., J., 2016, *Mechanical behavior and deformation kinetics of gradient structured Cu-Al alloys with varying stacking fault energy*, Journal of Alloys and Compounds, 687, pp. 152-160.
26. Huang, C.X., Hu, W., Yang, G., Zhang, Z.F., Wu, S.D., Wang, Q.Y., Gottstein, G., 2012, *The effect of stacking fault energy on equilibrium grain size and tensile properties of nanostructured copper and copper-aluminum alloys processed by equal channel angular pressing*, Materials Science and Engineering: A, 556, pp. 638-647.
27. Thévenot, F., 1990, *Boron carbide—A comprehensive review*, Journal of the European Ceramic Society, 6(4), pp. 205-225.
28. Shibata, S., Taya, M., Mori, T., Mura, T., 1992, *Dislocation punching from spherical inclusions in a metal matrix composite*, Acta Metallurgica et Materialia, 40(11), pp. 3141-3148.
29. Gao, H., Huang, Y., 2001, *Taylor-based nonlocal theory of plasticity*, International Journal of Solids and Structures, 38, pp. 2615-2637.
30. Greenwood J.A., 2020, *Metal transfer and wear*, Frontiers in Mechanical Engineering, 6, article 62.
31. Balokhonov, R.R., Evtushenko, E.P., Romanova, V.A., Schwab, E.A., Bakeev, R.A., Emelyanova, E.S., Zinovyeva, O.S., Zinovyev, A.V., Sergeev, M.V., 2020, *Formation of bulk tensile regions in metal matrix composites and coatings under uniaxial and multi-axial compression*, Physical Mesomechanics, 23, pp. 135-146.